Seismic Response Control for High-Rise Buildings Using Energy-Dissipation Devices†

KAMURA Hisaya[*1] NANBA Takayuki[*2] OKI Koji[*3] FUNABA Taku[*4]

Abstract:

Application of energy dissipation devices is reasonable and cost effective to maintain main structural members in elastic state for high-rise buildings. This paper discusses required energy dissipation performance for the longperiod ground motion on M7 class earthquake and the ability of JFE hysteretic energy dissipation devices.

1. Introduction

Seismologists have recently warned of the strong likelihood that Japan will suffer an M7-class large earthquake at some point in the next three decades. If this happens, it will be particularly important to maintain the building functions of high-rise buildings after the quake[1].

JFE Steel has reached the commercial stage in the development of extra-mild steels such as an ultralow-yield-point steel (JFE-LY100) and low-yield-point steel (JFE-LY225) for hysteretic dampers, as well as three types of vibration dampers: a buckling-restraint brace type, a wall-panel type, and a stud-panel type[2]. We have also developed hysteretic and visco-elastic hybrid damper, though not yet to the point of commercialization. This paper describes important points to keep in mind in the structural design of vibration damping structures applied to recent high-rise buildings, and outlines the structural performance of the vibration dampers developed at JFE Steel. We also evaluate the performance of vibration dampers installed in high-rise buildings against long-period earthquake motions[3], and give examples of the application of JFE vibration dampers to high-rise buildings.

2. Vibration Dampers and Structural Design of High-Rise Buildings

2.1 Recent Trend in Structural Design of High-Rise Buildings

The structural design of a high-rise building reduces the plasticization and input energy during an earthquake by assigning a relatively large elastic limit to the main frame and lengthening the natural period at a safety limit, respectively, by means of use of relatively smaller section. Through these steps, we can perform examinations in pursuit of both economical rationality and seismic safety[4]. To meet these conditions, architects tend to rely on high-tensile steel materials. This can be disadvantageous, however, as the decreased stiffness of frames made from high-tensile steel materials tends to compromise occupant comfort during strong winds. Vibration damping structures using energy-dissipation devices are often adopted to meet safety requirements during earthquakes while improving economic efficiency and occupant comfort during strong winds.

According to the results of hearings at major design offices and structural design departments of general contractors, energy-dissipation devices of various kinds are now installed in almost all high-rise, steel-frame buildings of 60 m or more in height, and hysteretic dampers are rated as the best energy-dissipation devices in terms of cost performance. Steel materials such as low-yield-

† Originally published in *JFE GIHO* No. 21 (Aug. 2008), p. 31–41

[*1] Dr. Eng.,
Senior Researcher General Manager,
Civil Engineering Res. Dept.,
Steel Res. Lab.,
JFE Steel

[*2] Senior Researcher Deputy Manager,
Civil Engineering Res. Dept.,
Steel Res. Lab.,
JFE Steel

[*3] Staff Deputy Manager,
Construction Engineering Services Dept.,
Construction Materials & Services Center,
JFE Steel

[*4] Staff,
Market Development Sec.,
Building Structure Engineering (East) Dept.,
JFE Engineering

point steel are used in 70% of energy dissipation members in dampers. LY225, a grade with relatively small strain hardening and strain rate dependence, accounts for about 90% of the steel used for dampers.

Among hysteretic dampers, the buckling-restraint brace type is the most frequently used. The wall-panel type is often constrained by building plans. Though the yield strength of the wall-panel type can be easily increased, the wall-panel structure cannot easily provide openings. The stud-panel type, on the other hand, provide openings readily. Yet as to be described later, stiffness decreases due to the effect of the bending deformation of the members supporting the damper and the beam members attached. In spite of this, the last three years have seen the increasing adoption of the stud-panel type in residential RC high-rise buildings, structures that have relatively rigid beam compared with steel structures and must be designed with passages and other types of openings. The buckling-restraint brace type seems to be studied as a hysteretic damper with balanced properties from these standpoints.

2.2 Design Method for an Effective-Moment-Resistant Frame with a Hysteretic Damper

Figure 1 shows the restoring characteristics of a moment-resistant frame (MRF) with a hysteretic damper. An MRF with a hysteretic damper is divided into a main frame consisting of columns and beams, and a damper portion consisting of a damper with connecting and supporting members. The shearing springs replacing the main frame and the damper portion are presumed to have the restoring characteristics of a complete elasto-plastic type. The ordinate of the restoring characteristics of an MRF with a hysteretic damper shown in **Fig. 1** represents the story shear force Q, and the abscissa represents the inter-story displacement δ. β is an index of yield shear force of the damper and expresses the contributional ratio of the damper portion to the maximum story shear force Q_u of the whole system. ψ, or the "trigger level coefficient," is an index of the story shear force

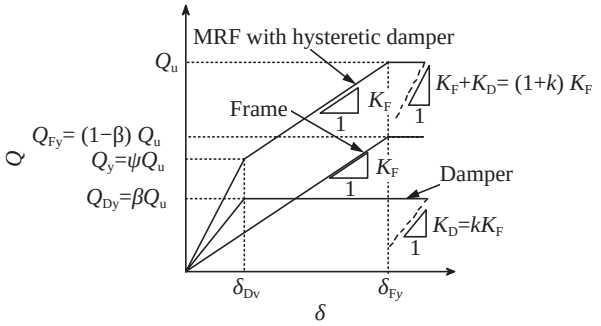

Fig. 1 Restoring characteristics of MRF with hysteretic damper

of the whole system when the damper portion starts to dissipate energy. The ratio of the elastic stiffness K_D of the damper portion to the elastic stiffness K_F of the main frame is referred to as the "stiffness ratio k." The stiffness ratio k expresses the contributional ratio of the shear force of the damper portion and the frame in the elastic region. In the calculation of K_D, we need to consider a deformation component due to the axial expansion and contraction of a column adjacent to the damper portion.

The condition under which the damper portion of a hysteretic damper yields prior to the main flame, i.e., the condition under which a hysteretic damper holds, is $\delta_{Dy} < \delta_{Fy}$. Hence, the contributional ratio of the yield strength β of the damper portion must satisfy the following equation[5]:

$$\beta < {}_U\beta = \frac{k}{1+k} \quad \cdots\cdots (1)$$

where ${}_U\beta$ is an upper limit value of the contributional ratio of yield strength β of the damper portion.

The following has been proposed as the optimum value for β_{opt} of the contributional ratio of yield strength β of the damper portion, on the precondition that the plastic deformation of the main frame is slight[6]:

$$\beta_{opt} = \frac{k}{1+k+2\sqrt{1+k}} \quad \cdots\cdots (2)$$

The following has been proposed as the range in which a damper portion can be expected to confer an effective hysteresis damping effect[7]:

$$0.1 \le \beta \le {}_U\beta_{opt} = 1 - \frac{1}{\sqrt{1+k}} \quad \cdots\cdots (3)$$

The results of seismic response analyses have verified that the displacement response becomes minimal when β is in the vicinity of β_{opt}, and that the hysteresis damping effect of the damper portion tends to decrease gradually when β exceeds ${}_U\beta$ [8,9].

The values of Eqs. (1) to (3) are shown in **Fig. 2**. Because the stiffness ratio k is preferably in the range of 0.5 to 2, the contributional ratios of yield strength for each story can clearly be set in the range of 0.1 to 0.3 according to the stiffness ratio, k.

Because the damper yields earlier than the main frame, we also need to consider the yield strength increase due to strain hardening after plasticization.

The upper limit value of damper steel materials is assumed to be the median of a specified maximum yield strength, i.e., 250 N/mm^2 for LY100 and 350 N/mm^2 for LY225. The material standard strengths of LY100 and

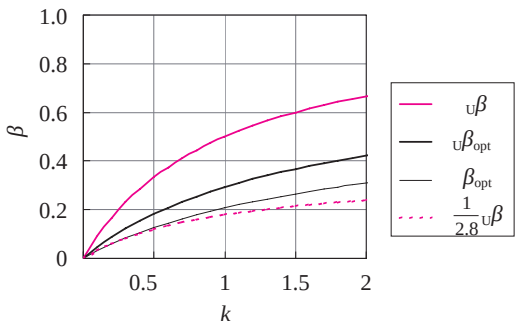

Fig. 2 Relationship of β To k

LY225 can be considered 88 N/mm^2 and 225 N/mm^2, respectively, hence yield strength increases of about 2.8 times and 1.6 times can be expected for a damper using LY100 and a damper using LY225, respectively. In consideration of the yield strength increase of LY100, Fig. 2 also plots the values obtained by multiplying the upper limit value of the contributional ratio of damper yield strength by 1/2.8. This value takes on numerical values relatively close to β_{opt} in the range up to k = 2. That is, the damper will not lose the hysteresis damping effect early if the contributional ratio of the yield strength β of the damper is set at a value less than β_{opt} according to k.

From the foregoing, we might assume that if the damper yield strength on each story is set at a value of not more than β_{opt}, we would not need to consider a yield strength increase of the damper. With a damper steel material with relatively small strain hardening, such as LY225, the yield strength increase due to strain hardening has only a small effect even when the contributional ratio β of the damper yield strength is set at a value in the vicinity of ${}_U\beta$.

2.3 Elastic Stiffness of Hysteretic Damper System

As described above, the design of a moment-resistant frame with a hysteretic damper requires that we appropriately set the yield strength and stiffness of a hysteretic damper and supporting members (a “damper system”) on each story in the main frame. The yield strength of a damper system can be evaluated in a simple manner as a shear force acting on the damper system when the damper yields. Yet in the case of a high-rise building, the stiffness of the damper system is greatly affected by the total bending deformation due to the expansion and contraction of columns supporting the damper. This calls for great care in evaluating the stiffness of the damper system.

A method for analytically evaluating the effect is described below.

Figure 3 shows the elastic stiffness K_{Di} of the damper system of an i-th story by taking the shear deformation component ${}_S\delta_{yi}$ during the damper yielding of the i-th story and the bending deformation component ${}_M\delta_{yi}$ due to the axial expansion and contraction of columns of a damper-installed span as examples. Q_{Dyi} is the yield shear force of the damper system. H_i denotes the story height. If ${}_M\delta_{yi}$ is ignored, the elastic stiffness of the damper system becomes ${}_SK_{Di}$. In actuality, however, the apparent stiffness decreases to ${}_MK_{Di}$ due to ${}_M\delta_{yi}$.

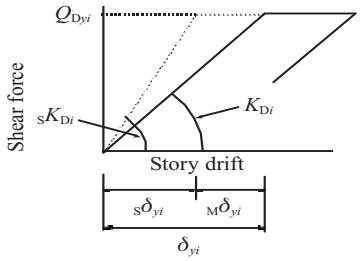

Fig. 3 Elastic stiffness of hysteretic damper system

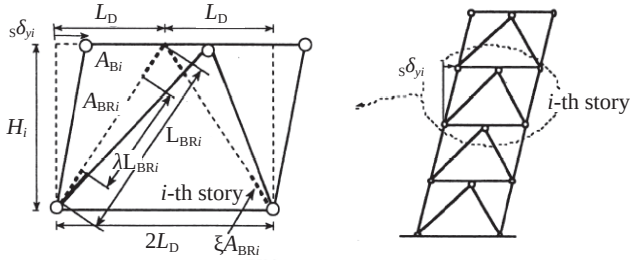

(a) Shear deformation component

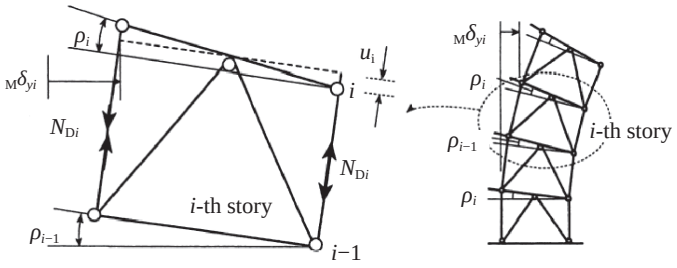

(b) Bending deformation component

Fig. 4 Deformation components of hysyteretic damper system

As shown in **Fig. 4**, the elastic stiffness ${}_SK_{Di}$ related to ${}_S\delta_{yi}$ in the case of a buckling-restraint brace is expressed by the following equations, in consideration of the axial expansion and contraction of the brace and beam:

$$ {}_SK_{Di} = \frac{2}{\dfrac{L_{BRi}^3}{EA_{BRi}^{eq}L_D} + \dfrac{L_D}{EA_{Bi}}} \quad \cdots\cdots (4) $$

$$ A_{ep}^{BRi} = \frac{A_{Bi}}{\lambda + \dfrac{1-\lambda}{\xi}} \quad \cdots\cdots (5) $$

where, L_{BRi} and λL_{BRi} denote the total brace length of the i-th story and the nominal damper length without the

length of the elastic connecting section, respectively; A_{BRi} and ξL_{BRi} denote the sectional area of the brace and the sectional area of the connecting section, respectively; A_{BRi}^{eq} denotes the equivalent sectional area of the brace; $2L_D$ denotes the length of the span over which the damper is installed; A_{Bi} denotes the sectional area of the upper floor beam of the i-th story; and E denotes Young's modulus.

As shown in Fig. 4(b), a relative rotational angle of ρ_i is generated in the floor beams of the i-th story. ${}_M\delta_{yi}$ is expressed as follows using this ρ_i:

$$ {}_M\delta_{yi} = \sum_{k=1}^{i-1} \rho_k H_k \quad \cdots\cdots (6) $$

An additional axial force N_{Di} is applied to the column, and the column expands and contracts as shown in Fig. 4(b). The amount of expansion and contraction u_i of the column of the i-th story is expressed by the following equations:

$$ u_i = \frac{N_{Di} H_i}{E A_{ci}} \quad \cdots\cdots (7) $$

$$ N_{Di} = \frac{1}{2L_D} \sum_{j=i+1}^{N} Q_{Dyi} H_j \quad \cdots\cdots (8) $$

where A_{ci} denotes the sectional area of the column adjacent to the damper of the i-th story.

Using u_i of Eq. (7), we obtain the relative rotational angle ρ_i from the following equation:

$$ \rho i = \frac{u_i}{L_D} \quad \cdots\cdots (9) $$

Therefore, ${}_MK_{Di}$ is expressed as follows:

$$ {}_MK_{Di} = \frac{Q_{Dyi}}{\dfrac{H_i}{EL_D} \displaystyle\sum_{k=1}^{i-1} \frac{N_{Dk} H_k}{A_{Ck}}} \quad \cdots\cdots (10) $$

We obtain the elastic stiffness K_{Di} of the damper system of the i-th story from Eqs. (4) and (10). In the case of an inverted K type, where buckling-restraint braces intersect each other at one point on a lower beam of the i-th story, we can make the calculations by changing $i + 1$ of Eq. (8) to i.

Figure 5 shows the stiffness of a damper system of an eight-story frame designed using buckling-restraint braces and stud-panel type dampers in two cases: once with the total bending deformation taken into account, and once with the total bending deformation ignored. As the figure clearly shows, the stiffness of the damper system of the buckling-restraint brace is two or three times as high as that of the stud-panel type. Even in the eight-story building, the apparent stiffness in the upper part of the building decreases to less than one-half of that when the effect of the total bending deformation is ignored. We thus find that the buckling-restraint brace is greatly influenced by the total bending deformation due to the axial expansion and contraction of the column, and that the stud-panel type damper is greatly influenced by the elastic deformation of the supporting members of shear panels and attached beams.

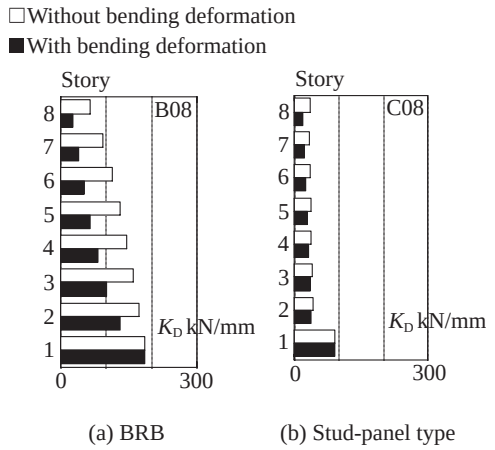

Fig. 5 Elastic stiffness distribution of hysteretic damper system

3. JFE's Vibration Damping Devices

3.1 Structural Types of Hysteretic Damper

JFE produces hysteretic vibration dampers of the three structural types (the brace type, the assembled stud-panel type, and the wall type) shown in **Fig. 6**. Extra-mild steels are used in the plasticized parts of each (SN400 grade steel is also used in the brace type).

3.2 Restoring Force and Fatigue Characteristics of Shear-Yielding Type Dampers

In shear-yielding type vibration dampers (the wall type and the assembled stud-panel type), the steel grade and width-thickness ratio of the damper steel used in the panel part both have influences on the hysteretic characteristics and amount of energy dissipation of the damper. To ensure sufficient energy dissipation characteristics

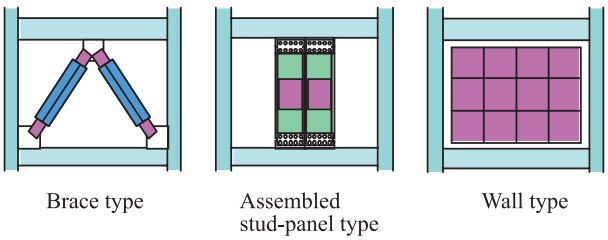

Fig. 6 JFE Hysteretic Damper

during an earthquake, we need to grasp the fatigue characteristics associated with the small-amplitude cyclic loading generated by wind loads and the large-amplitude cyclic loading during large earthquakes.

We confirmed the performance of the shear-yielding type vibration dampers by performing two types of tests. First, we performed the loading test with progressively higher loads using three parameters: the steel grade, the width-thickness ratio, and the loading rate. Second, we performed the low-cycle fatigue test performed using two parameters: the steel grade and the loading amplitude. To test the performance of the shear panel, we applied a load via displacement control of a 150-t actuator with the loading device shown in **Fig. 7**. For the load test with progressively higher loads, the waveform of the dynamic test was a sine wave of 2 Hz and the waveform of the static test was a triangular wave of 0.5 mm/s. After amplifying the amplitude proportionally from 1/800 rad to 6/100 rad, the amplitude of 6/100 rad was repeated until cracks passed through the panel part. In the low-cycle fatigue test, cyclic loads were applied until the yield strength decreased to 95% of the maximum yield strength, or until cracks passed through. The restoring characteristics and fatigue characteristics obtained from the results of the series of tests are described below.

Based on the results of the static loading test with progressively higher loads, we tried to model the hysteresis for each steel grade and each width-thickness ratio. Though Ramberg-Osgood type models have generally been proposed, we used tri-linear type modeling in this study, in consideration of the universality and the ease of design. **Figure 8**(a) shows modeling with LY225, as an example. Errors appear because the rise gradient of the experiment decreases as the loading amplitude rises. Yet loops quite similar to each other are plotted. Furthermore, as shown in Fig. 8(b), the experiment and the calculation are almost in agreement at low amplitudes, in terms of the cumulative ductility factor. The energy dissipation of the hysteresis model is evaluated at about 90%, and the value tends to fall further as the shear drift angle increases.

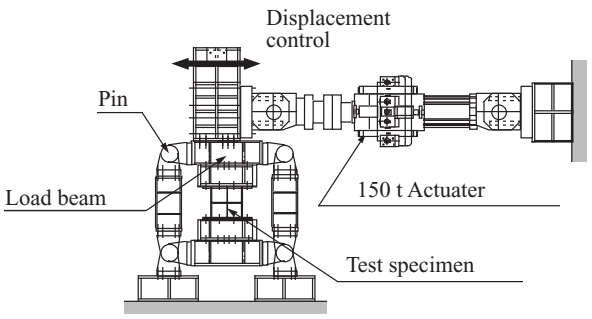

Fig. 7 Setup of shear panel test

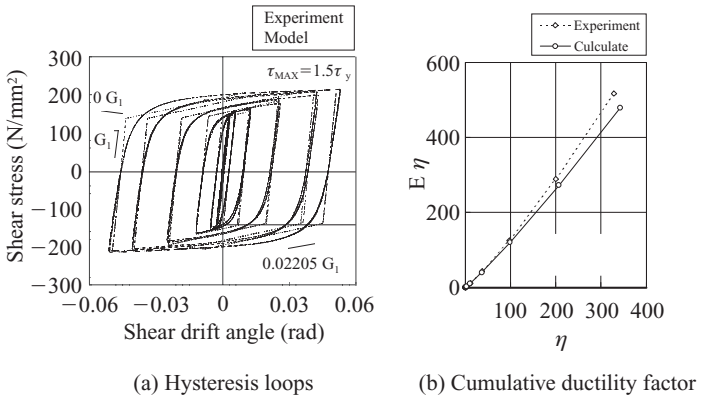

(a) Hysteresis loops (b) Cumulative ductility factor

Fig. 8 Comparison of model for experiment (LY225)

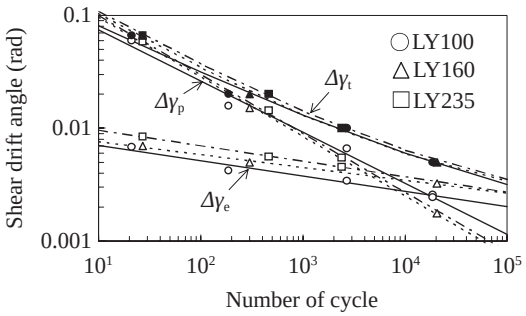

Fig. 9 Relation of fatigue life

Figure 9 shows the relation of the number of cycles to the total loading amplitude of each steel grade in the results of the fatigue test for the shear panel. Incidentally, the number of cycles N adopted is the number of cycles obtained when the yield strength decreased to 95% of the maximum yield strength. Both the elastic strain $\Delta\gamma_e$ and plastic strain $\Delta\gamma_p$ can be approximated by a straight line, and the Manson-Coffin rule holds. The test results for LY100 were obtained from the assembled type, hence the plastic strain tends to rise to somewhat high levels at low amplitudes as a result of the difference in constraint conditions. On the whole, however, LY225 has a long fatigue life, exhibiting a tendency about the same as that observed in the material test results. With repetitive application with a loading amplitude of not more than about 0.01 rad, the fracture mode provides weld cracks, hence we ultimately find little difference between the steel grades.

The fatigue life curve is expressed by the following equation for each steel grade:

$$\Delta\gamma_t = \Delta\gamma_p + \Delta\gamma_e$$
$$= 0.211 \cdot (N_{95}) - 0.453 + 0.010 \cdot (N_{95}) - 0.136 \quad \text{(LY100)}$$
$$= 0.335 \cdot (N_{95}) - 0.523 + 0.013 \cdot (N_{95}) - 0.138 \quad \text{(LY225)} \qquad \cdots\cdots\cdots (11)$$

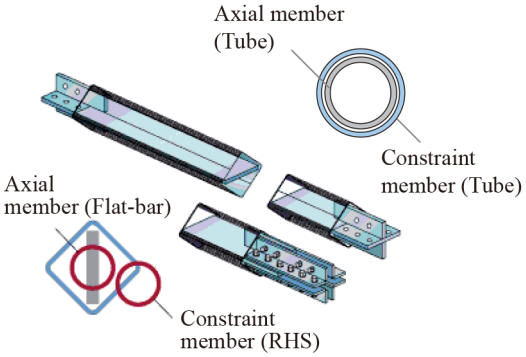

Fig. 10 Buckling restraint braces by tube

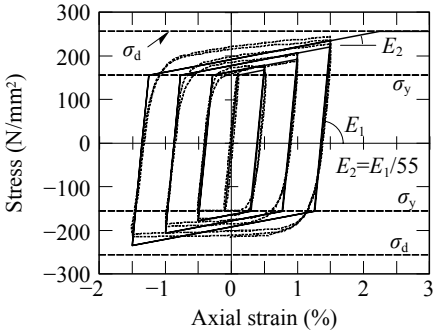

Fig. 11 Evaluation of hysteretic loop model

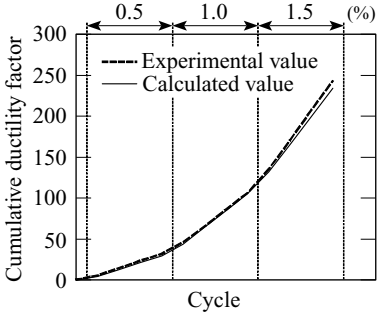

Fig. 12 Comparison of cumulative ductility factor

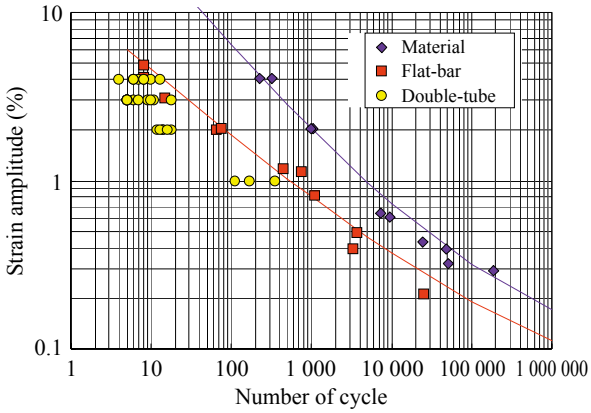

Fig. 13 Fatigue characteristic of BRB

3.3 Restoring Force and Fatigue Characteristics of Brace-Type Dampers

Various strategies entailing the use of RC members, steel tube concrete, shapes, etc. have been proposed for the buckling-restraint method for the axial members of the brace[10]. Two points are to be considered for the construction and design of buckling-restraint braces:

(1) The yield strength and stiffness are sufficient to prevent the buckling of the axial member.
(2) The plastic contraction allowance of the axial member is ensured, and insulation is used to prevent the friction and adherence of the axial member and the restraining member.

Any buckling-restraint method for the axial member of the brace may be adopted, provided that both of these points are ensured. The steel tube JFE uses as the brace-type damper serves as a buckling-constraint member that requires no special insulation (**Fig. 10**). The two points described above are ensured by appropriately setting the width-thickness ratio, diameter-thickness ratio, and clearance of the axial member and constraint steel tube.

The authors has conducted the following experiments to grasp the conditions necessary to ensure that this brace will exhibit sufficient performance as a damping member:

(1) Cyclic loading experiment with a brace as a single member with variation in the following parameters: the mechanical properties of the axial member, the slenderness ratio of the auxiliary steel pipe, the width-thickness ratio of the axial member, the diameter-thickness ratio of the auxiliary steel tube, and the clearance between the axial member and the auxiliary steel tube
(2) Partial frame experiment to grasp the applicability to an actual structure and the hysteresis characteristics as a moment restraint frame with a brace
(3) High-speed loading experiment with the actual seismic ground motions considered
(4) Fatigue characteristics experiment

In this section we describe the modeling of hysteresis loops and the fatigue characteristics. To obtain as simple an expression as possible, we perform the modeling using a tri-linear model in which the yield strength (σ_y) and the yield strength after strain hardening (σ_d) provide break points. **Figure 11** shows a hysteresis loop model of LY225. **Figure 12** compares experimental and calculated values of the changes in the cumulative ductility factor resulting from the strain dissipation energy. The calculated and experimental values for the cumulative ductility factor correspond well, though the former are a little lower than the latter. This model therefore appears to sufficiently serve its purpose.

Figure 13 shows results of a fatigue rest conducted on test specimens using LY100 and LY225 as axial members and materials. The axial members have the sectional shapes of flat bars and circular tubes. The ordinate in the figure denotes the total strain range, and

the number of cycles adopted is the number of cycles obtained when the tension-side peak load decreases to 95% of the load in a stable state.

The figure also shows the results of flat bar (LY100) by the following equation as an example of a fatigue life curve:

$$\Delta\varepsilon_t = \Delta\varepsilon_p + \Delta\varepsilon_e$$

$$= 0.112\,8 \cdot (N_{95})^{-0.412\,9} + 0.002\,96(N_{95})^{-0.100\,1} \quad \cdots\cdots\cdots (12)$$

We thus find that if the buckling-constraint member of a brace type damper is appropriately designed, the prescribed deformability will be obtained irrespective of the axial sectional shape.

4. Evaluation of the Performance of Dampers against Long-Period Seismic Ground Motions

4.1 Long-Period Seismic Ground Motions by Ocean-Trench Earthquakes

Ocean-trench massive earthquakes are characterized by an abundance of long-period components and long duration times. Their epicenters are positioned off of Tokai, Tonannkai, Nannkai, etc. These earthquakes pose serious threats to high-rise buildings and like structures with long natural periods. The dampers for these structures must therefore perform especially well.

In this section we evaluate whether the above-described tube-in-tube type brace can be expected to meet the performance requirements in the event of a massive ocean trench earthquake. We begin by preparing a model of a high-rise building of a type thought to be greatly influenced by massive ocean-trench earthquakes, then perform a time history response analysis with the OSA-NS waves (simulated waves)[11] of an ocean-trench earthquake and determine the required performance of the damper based on our analytical results. Next, we conduct a dynamic experiment in which the structural response waves obtained by the above-described time history response analysis are imposed on the tube-in-tube type brace. We derive the actual performance from the results of the experiment and compare it with the calculated required performance.

4.2 Required Performance of Hysteretic Dampers

4.2.1 Input seismic waves and analytical model

The analytical model was a 40-story building of a steel construction, with analytical model damping braces

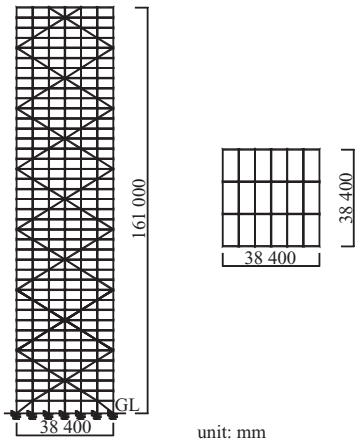

Fig. 14 Analytical model

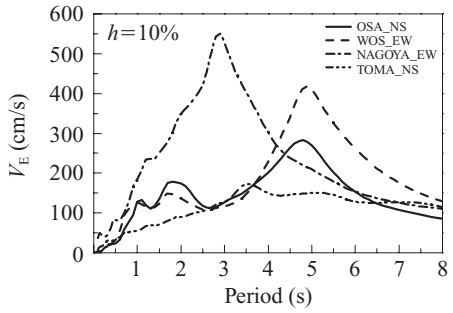

Fig. 15 Energy spectrum

arranged in an X shape (**Fig. 14**). The story height is 5 m for the first floor and 4 m for every floor above it. The planar shape is the same for all stories. The member construction consists of 600 × 600 mm columns with box-shaped sections with plate thicknesses of 35 to 55 mm, and girders 700 to 800 mm in depth and 200 to 250 mm in width with H-shaped sections with flange thicknesses of 14 to 28 mm. The damping constant is 2%. The degree of yield stress of the axial member of the brace is 100 N/mm^2 and the distribution conforms to an optimum distribution of the yield shear force coefficient based on the damper yield strength of the first story. We set the primary natural period of a model of the frame alone at T_1 = 4.64 s. **Figure 15** shows the energy spectra of long-period seismic ground motions after references 3) and 11). We use the OSA-NS wave in this analysis.

4.2.2 Analysis results

We perform a time history response analysis using the yield shear force coefficient ${}_s\alpha_{y1}$ of the damping brace of the first story as a parameter. **Figure 16** shows acceleration-converted energy input V_E, and **Fig. 17** shows the ratio of the energy dissipation of the damping brace to the input energy. From Fig. 16 we obtain V_E = 200 to 280 cm/s, and this energy input agrees substantially with the V_E shown in Fig. 15. From Fig. 17 we obtain ${}_s\alpha_{y1} = 12 \times 10^{-3}$ as optimum value, where the

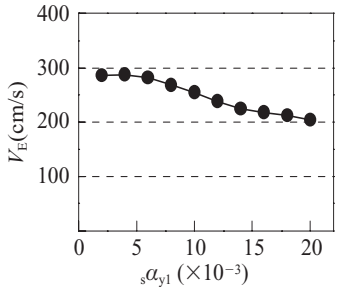

Fig. 16 V_E vs. $_s\alpha_{y1}$

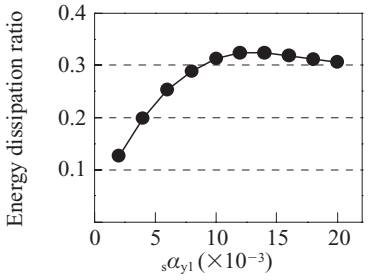

Fig. 17 Energy dissipation ratio vs. $_s\alpha_{y1}$

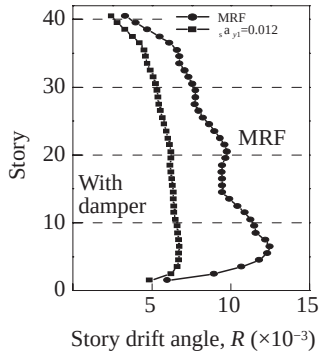

Fig. 18 Distribution of story drift angle

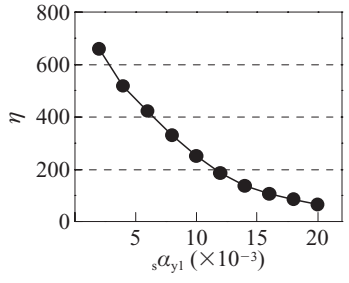

Fig. 19 η vs. $_s\alpha_{y1}$

value at which the energy dissipation ratio is regarded as local maximum[12]. **Figure 18** shows the story distribution of the maximum story drift angle R. When $_s\alpha_{y1}$ = 12 × 10^{-3}, R is within 1/100 even in the seventh story, where the maximum drift angle is the largest. **Figure 19** shows the cumulative ductility factor η[13] of the damping brace of the seventh story. The value of $_s\alpha_{y1}$ declines as the value of η increases, and η_d = 186.3 when $_s\alpha_{y1}$ is optimal. The cumulative plastic strain energy W_p per damping brace at this point is W_{pd} = 834.1 kN·m, and the yield strength N_y is N_{yd} = 1 658.2 kN. If we select the axial-load-carrying tube from the 100 N/mm^2 class low-yield-point steel tubes with a slenderness ratio λ of 120 or less and a diameter-thickness ratio of 15, the size of the tube available from among standard JFE sizes is ϕ 298 × 19.9. On the assumption that both ends are provided with a 1-m connecting section, however, we set the axial-load-carrying tube length at 5.5 m.

For the analysis results, the maximum value η_{dmax} of η was 658.6 kN·m and that of W_{pdmax} was 491.5 kN·m at $_s\alpha_{y1}$ = 12 × 10^{-3}.

4.3 Performance of the Hysteretic Dampers

4.3.1 Outline of experiment

The test specimen used in the experiment is a tube-in-tube type buckling-restraint brace (inner-tube restraint type) in which both ends are pin connected. A 100 N/mm^2 class low-yield-point steel tube (JFE-LY100) with a diameter-thickness ratio of 15 is used as the axial-load-carrying tube, and an ordinary steel tube is used as the constraint tube. Details of the test specimen are shown in **Fig. 20**.

The load is imposed by repeatedly inputting the input wave described below until the test specimen is broken. For comparison with the required capacity under an increasingly severe condition for response, we performed a time-history-response analysis with a model of a frame alone and prepared the input wave based on the horizontal displacement response wave of the 7th story with the story drift angle set at maximum. First, we converted the horizontal displacement response wave

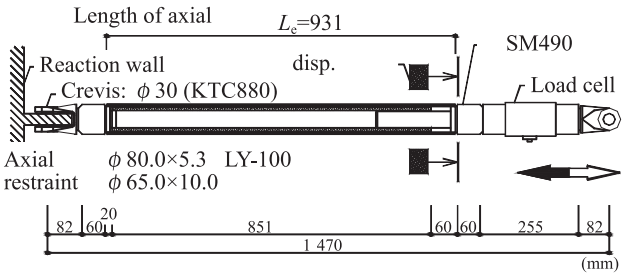

Fig. 20 Testing specimen

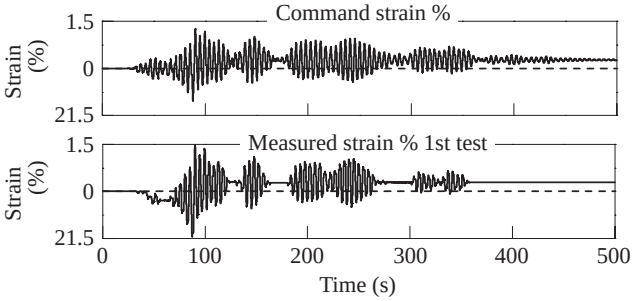

Fig. 21 Time history of strain of hysteretic damper

into an axial displacement wave of the damping brace and corrected for the different lengths of the axial-load-carrying tubes of the test specimen and brace. The actually inputted wave (the first wave) is shown in **Fig. 21**. The amplitude ratio on the ordinate, a value obtained by dividing the input relative displacement by the length of the axial-load-carrying tube, is equivalent to the strain amount of the axial member of the brace. The experimental design is clearly appropriate when we consider the significant effect of the high-amplitude ratios on the energy dissipation of the damper.

4.3.2 Experimental results and discussion

Loading was performed 10 times in all. We observed a decrease in the yield strength and fractures during the tenth loading, and therefor decided to end the experiment.

Photo 1 shows the condition of the final fracture. Buckling occurred at an end portion of the brace test specimen, and a crack occurred in the valley portion of the buckling, leading to the fracture.

Table 1 shows results of the loading performed each time. The cumulative ductility factor η decreases a little as the number loads increases. We speculate that this was the result of a decrease in the stiffness of the brace caused by an accumulation of local buckling in the end portion of the test specimen.

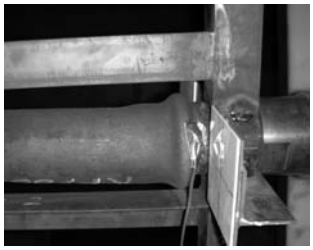

Photo 1 Failure mode

Table 1 Testing results

Number	Maximum stress (N/mm²)		Dissipation energy (kNm)	Cumulated ductility factor, η
	plus	minus		
1	214	201	105	1 863
2	222	204	103	1 829
3	224	206	102	1 813
4	228	206	102	1 799
5	226	206	101	1 783
6	228	206	100	1 774
7	227	206	99	1 757
8	228	207	98	1 740
9	231	206	97	1 724
10	236	203	92	1 628
		Sum.	1 000	17 709

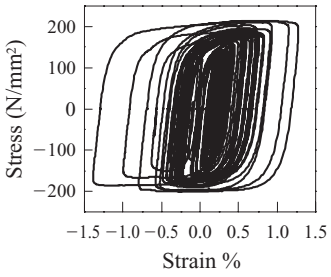

Fig. 22 Stress-strain relation

Figure 22 shows the stress-strain relation of the first wave. Here we find that stable hysteresis loops are drawn even though the maximum stress intensity increases due to the effect of strain hardening. We calculate the cumulative ductility factor η of the test specimen by adding the values obtained each time, as shown in Table 1. The result becomes η_c = 16 081.1. W_{pc} at this point is 908.4 kN·m, and N_{yc} is 124.4 kN. To keep the assumptions conservative, however, we exclude the value that led to the fracture in the tenth loading. η_c is about 86.3 times the value of η_d found in the analysis, and the tube-in-tube brace in question has sufficient performance. For η_{dmax} also, we provide an allowance of approximately 24.4 times. And for the maximum V_E, of 550 cm/s assumed from Fig. 15, η_{dmax} is 2432.2 and η_c has a margin of approximately 6.6 times.

5. Energy-Dissipation Devices for Both Wind-Resistant and Earthquake-Resistant Purposes

5.1 Out Live of Test Speciment and Experiment

This section describes the performance evaluation of a hybrid damper of the partial damping wall type now being developed at the JFE Steel (**Fig. 23**, **Photo 2**). This hybrid damper is composed of a visco-elastic damper designed for wind response connected in a series-parallel manner with a hysteretic panel

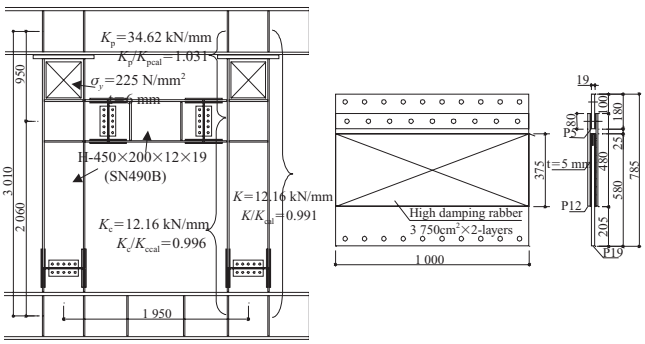

Fig. 23 Hysteretic and visco-elastic hybrid damper

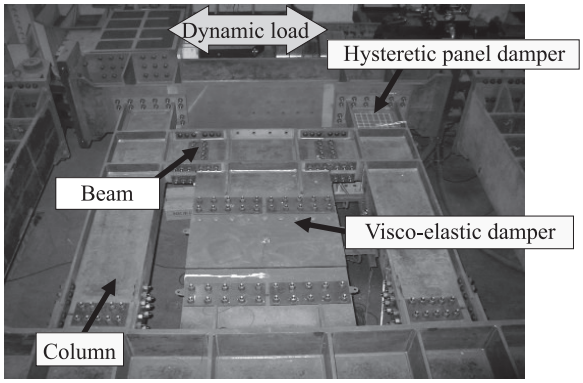

Photo 2 Testing set-up of hybrid damper

damper effective in seismic response[14]. The hysteretic panel damper is composed of two studs and a horizontal member (both: H-450 × 200 × 12 × 19, SN490B9), with part of the web formed from a low-yield-point steel (t = 6 mm, σ_y = 225 N/mm^2). The visco-elastic damper is formed by stacking high-damping rubber (t = 5 mm) made by Yokohama Rubber Company, Ltd. in two layers. We call this hybrid damper a "series-parallel" type for two reasons: first, the damper is made up of two types of dampers; second, the visco-elastic damper is connected in series to a low-yield-point panel via a horizontal member and connected in parallel to the studs.

We tested this hybrid damper by subjecting it to dynamic loading at 0.3 and 1 Hz as shown in Photo 2. The amplitude used in the experiment is divided into small amplitudes (assumed for wind response) and large amplitudes (assumed for seismic response), with a story drift angle R of 1/500 (δ = 6 mm) serving as the boundary.

5.2 Experimental and Discussion

(a) **Figure 24** shows the restoring characteristics of the low-yield-steel panel of the hysteretic panel damper. The maximum displacement R_{pmax} of the panel is 1/16.9 rad and the yield strength decreases due to buckling. All parts of the studs and horizontal members remain within the elastic range even after the panel buckles, except for the parts in the vicinity of the damping constant at small amplitudes of 2 to 3%.

(b) **Figure 25** shows the damping ratio and constant of the visco-elastic damper. The ratio of the deformation of the high-damping rubber to the damper displacement (relative displacement between the horizontal members and the lower beam) is 75 to 90%. Though the stiffness of the high-damping rubber is almost the same as the stiffness obtained with the evaluation equation in reference[15], we use a value corrected for each cycle in the evaluation of the performance of the hybrid damper, to adjust for the slight cycle dependence. The damping constant is approximately 0.3.

(c) **Figure 26** shows examples of hysteresis loops of the hybrid damper at small amplitudes. The deformation of the high-damping rubber is approximately 60% of the story drift and the contributional ratio of yield strength is approximately 25%. The damping constant

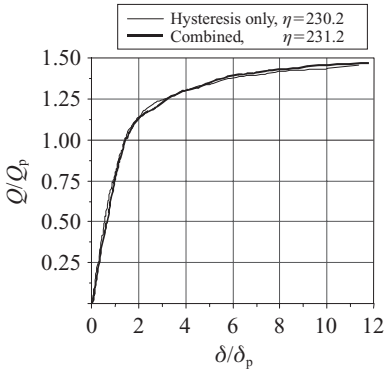

Fig. 24 Q-δ relation of hysteretic shear panel damper

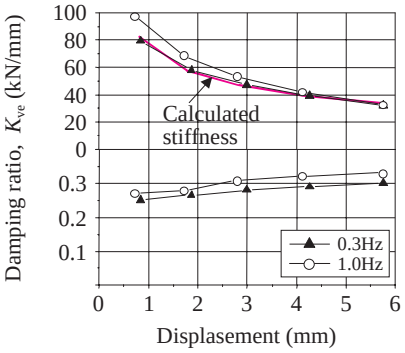

Fig. 25 Damping ratio-displacement relation of visco-elastoc damper

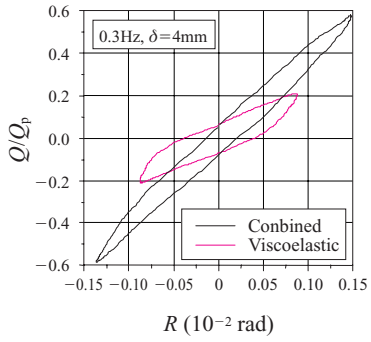

Fig. 26 Hysteresis loops of hybrid damper (Small amplitude)

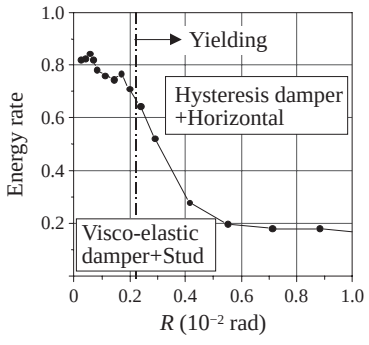

Fig. 27 Energy rate of hybrid damper due to story drift angle

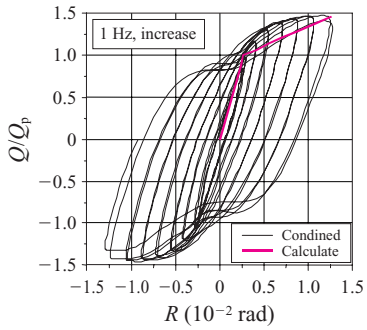

Fig. 28 Hysteresis loops of hybrid damper (Large amplitude)

of the hybrid damper is 6 to 7%. At R = 1/500 or less, the hysteretic panel damper is elastic and mainly the visco-elastic damper dissipates energy (**Fig. 27**).

(d) **Figure 28** shows hysteresis loops of the hybrid damper at large amplitudes. R_{pmax} = 1/77.9 rad. The performance of the panel is the same as with the hysteretic panel damper alone shown in Fig. 24. The contributional ratio of energy dissipation of the panel increases with increasing amplitude (Fig. 27). The deformation of the high-damping rubber is suppressed to not more than 10 mm (γ = 200%), and no decrease in performance is observed. At R = 1/100, the energy dissipation capacity of the hysteretic panel damper increases by about 8% due to the effect of the visco-elastic damper.

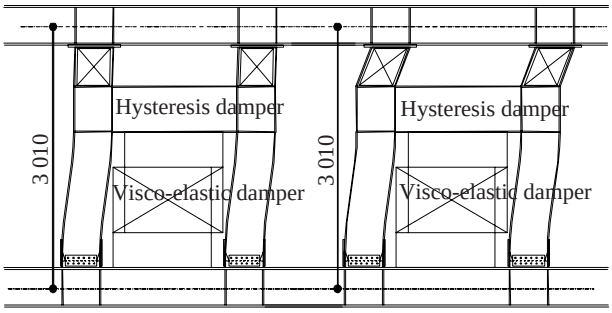

(a)Small amplitube (wind) (b)Large amplitube (earthquake)

Fig. 29 Energy dissipation mechanism of hybrid damper

As shown in **Fig. 29**, the energy dissipation in the series-parallel hybrid damper is performed mainly by the visco-elastic damper at small amplitudes and by the hysteretic panel damper at large amplitudes. Hence, the series-parallel hybrid damper is effective for both wind response and seismic response. And at large amplitudes we can suppress the deformation of the visco-elastic damper to less than the elastic limit of the studs and improve the stiffness per unit area by making the visco-elastic damper thin.

6. Concluding Remarks

In this paper we described the trend in the applica-

Table 2 Example of buildings installed JFE hysteretic dampers

No.	Use	Number of story	Structural type	Material for dampers	Number of dampers	Damper type	Site
1	Office	12-story	Steel	LY100	118	BRB	Tokyo
2	Office	17-story	Steel	LY100	128	BRB	Tokyo
3	Office	28-story	Steel	LY100	156	BRB	Tokyo
4	Office	11-story	Steel	LY100	32	BRB	Tokyo
5	Office	26-story	Steel	LY100	340	BRB	Tokyo
6	Residence	40-story	RC	LY100	80	Stud-panel	Tokyo
7	Complex	25-story	Steel	LY225	380	BRB	Tokyo
8	Complex	13-story	Steel	LY225	112	BRB	Tokyo
9	Office	—	Steel	LY225	208	BRB	Okayama
10	Residence	31-story	RC	LY225	70	Stud-panel	Tokyo
11	Residence	30-story	RC	LY225	72	Stud-panel	Tokyo
12	Office	39-story	Steel	LY225	168	BRB	Tokyo
13	Residence	30-story	RC	LY160	444	Stud-panel	Kanagawa
14	Residence	58-story	RC	LY225, etc.	1 152	Stud-panel	Tokyo
15	Residence	59-story	RC	LY225	16	Stud-panel	Tokyo
16	Office	16-story	Steel	LY225	85	BRB	Osaka
17	Residence	40-story	RC	LY225	92	Stud-panel	Tokyo
18	Manufacturing	—	Steel	LY225, etc.	70	BRB	Tokyo
19	Office	23-story	Steel	LY100	28	BRB	Tokyo
20	Retrofits	8-story	Steel	LY225	—	BRB	Tokyo

BRB : Buckling restraint brace

Photo 3 Example of buildings installed JFE hysteretic dampers

tion of damping structures to recent high-rise buildings, important points to keep in mind in the structural design of damping structures, and an outline of the structural performance of JFE-developed vibration dampers. Further, we discussed the required and actual energy-dissipation performance of vibration dampers installed in high-rise buildings.

Lastly, **Table 2** and **Photo 3** show representative track records of the vibration dampers introduced in this paper, as observed over the past five years. As the table clearly illustrates, many of JFE's vibration dampers are adopted in RC high-rise buildings, as well as in steel-frame high-rise buildings. And the adoption of JFE vibration dampers in production facilities other than high-rise buildings is also increasing. Many predictions of damage due to massive earthquakes, such as inland earthquakes in the Tokyo Metropolitan Area, have been disclosed to the public in recent years. This is one of the reasons why seismic dampers are expected to become more widespread in various building applications in the years to come. JFE will take part in this trend by developing new vibration damping techniques to meet social needs in the future, as well.

Portions of the results of a research project conducted jointly with the Kitamura Laboratory, Structural Engineering, Department of Architecture, Faculty of Science and Technology, Tokyo University of Science are used in the study on the performance evaluation of dampers for long-period seismic ground motions described in Chapter 4. The authors would like to extend their thanks to the persons concerned.

References

1) Headquarters for Earthquake Research Promotion. "National Seismic Hazard Maps for Japan (2007)." 2007.
2) e.g., Ito, S.; Kamura, H.; Shimokawa, H.; Katayama, T.; Hirota, M.; Ueki, T. Hysteretic Energy Dissipation Devices with Low Yield Strength Steel for Passive Structural Control. NKK Technical Report. 2000, no. 170, p. 67–74.
3) Tsunoda, M.; Ishii, T.; Miyagawa, K.; Kitamura H. Evaluation On Performance Of Buckling-Restrained Tube-In-Tube Energy Dissipative Braces for the Long-Period Ground Motion. Summaries of Technical Papers of Annual Meeting Architectural Institute of Japan. C-1, 2006-07, p. 895–896.
4) Japanese Society of Steel Construction. Guidelines for Dynamic Seismic Design of Steel Frames Using CFT Columns. JSSC Technical Report. 2006, no. 76.
5) Inoue, K. Seismic Design of Structures with Hysteretic Damper, Proceedings of Symposium on a new course of Seismic Design. Architectural Institute of Japan. 1995, p. 95–111.
6) Building Research Institute and Japan Iron and Steel Federation. Seismic Design of Steel Structures with Hysteretic Damper. 2002.
7) Inoue, K.; Ono, S. Optimum Strength Ratio of Hysteretic Damper and Design Strength of Frames. Journal of Structural Engineering. 1995, vol. 41B, p. 9–15.
8) Kamura, H.; Inoue, K.; Kuwahara, S.; Ogawa, K. Modeling of the Moment Resistant Frame with Hysteretic Damper to Fishbone-Shaped Frame for the Response Analysis. Journal of Structural and Construction Engineering. Transactions of AIJ. 2002-12, no. 562, p. 151–158.
9) Ogawa, K. Residual Deformation of Steel Frames with Hysteretic Dampers. Journal of structural and construction engineering. Transactions of AIJ. 2001-01, no. 539, p. 151–158.
10) e.g., Maeda, Y.; Kamura, H.; Takeuchi, T.; Iwata, M.; Wada A. Fatigue Properties of Practical-Scale Unbonded Braces (Part 1, 2). Summaries of technical papers of Annual Meeting Architectural Institute of Japan. C-1, 1999, p. 813–814.
11) Kawabe, H.; Kamae, K.; Irikura, K. Strong Motion Simulation of Hypothetical Nankai Earthquake Using Characteristic Source Model. Proceedings of the 2002 Fall Meeting of Seismological Society of Japan. A31.
12) Atsumi, T.; Uramoto, H.; Ishii, M.; Kitamura, H. Vertical Distribution of Hysteretic and Velocity-Dependent Dampers for High-Rise Steel Structure. Summaries of Technical Papers of Annual Meeting Architectural Institute of Japan. B-2, 2006, p. 763–766.
13) Akiyama, H. Seismic Design of Buildings Based on Energy Balance. Gihodo Shuppan. 1999-11.
14) Hirota, M.; Katayama, T.; Kamura, H. Study on Shear Wall Damper connected H-Section Members Using Low Yield Strength Steel (Part 5–7). Summaries of Technical Papers of Annual Meeting Architectural Institute of Japan. C-1, 1998, p. 801–806.
15) Ishikawa, R.; Suwa, H.; Gokan, S.; Suzuki, T. A Study of Mechanical Model for Viscoelastic Damper (Part 1, 2). Summaries of Technical Papers of Annual Meeting Architectural Institute of Japan. B-2, 1999, p. 959–962.